Original Article

MOLECULAR METABOLISM

Deletion of the mitochondrial calcium uniporter in adipose tissue promotes energy expenditure and alleviates diet-induced obesity

Mengting Jia[2,5], Siqi Liu[1,5], Yang Xiao[1], Zhiwang Zhang[1], Mingming Li[1], Xinyu Qi[2], Xinyi Qi[2], Lin Yu[1], Caiyong Zhang[1], Tianyu Jiang[1], Tingli Pan[1], Yu Sun[1], Jingsu Yu[1], Songtao Su[1], Yixing Li[2], Turtushikh Damba[3], Khongorzul Batchuluun[4], Yunxiao Liang[1], Lei Zhou[1,*]

ABSTRACT

Objective: Studies have shown a correlation between obesity and mitochondrial calcium homeostasis, yet it is unclear whether and how *Mcu* regulates adipocyte lipid deposition. This study aims to provide new potential target for the treatment of obesity and related metabolic diseases, and to explore the function of *Mcu* in adipose tissue.

Methods: We firstly investigated the role of mitoxantrone, an *Mcu* inhibitor, in the regulation of glucose and lipid metabolism in mouse adipocytes (3T3-L1 cells). Secondly, C57BL/6J mice were used as a research model to investigate the effects of *Mcu* inhibitors on fat accumulation and glucose metabolism in mice on a high-fat diet (HFD), and by using CRISPR/Cas9 technology, adipose tissue-specific *Mcu* knockdown mice ($Mcu^{fl/+}$ AKO) and *Mcu* knockout of mice ($Mcu^{fl/fl}$ AKO) were obtained, to further investigate the direct effects of *Mcu* on fat deposition, glucose tolerance and insulin sensitivity in mice on a high-fat diet.

Results: We found the *Mcu* inhibitor reduced adipocytes lipid accumulation and adipose tissues mass in mice fed an HFD. Both $Mcu^{fl/+}$ AKO mice and $Mcu^{fl/fl}$ AKO mice were resistant to HFD-induced obesity, compared to control mice. Mice with $Mcu^{fl/fl}$ AKO showed improved glucose tolerance and insulin sensitivity as well as reduced hepatic lipid accumulation. Mechanistically, inhibition of *Mcu* promoted mitochondrial biogenesis and adipocyte browning, increase energy expenditure and alleviates diet-induced obesity.

Conclusions: Our study demonstrates a link between adipocyte lipid accumulation and mCa^{2+} levels, suggesting that adipose-specific *Mcu* deficiency alleviates HFD-induced obesity and ameliorates metabolic disorders such as insulin resistance and hepatic steatosis. These effects may be achieved by increasing mitochondrial biosynthesis, promoting white fat browning and enhancing energy metabolism.

Keywords *Mcu*; Obesity; Adipose tissue; Calcium homeostasis; Energy expenditure; Mitoxantrone

1. INTRODUCTION

Obesity is a metabolic disease of excessive fat accumulation as a result of an imbalance in energy intake and consumption [1]. It is associated with the development of several chronic diseases such as type 2-diabetes, non-alcoholic fatty liver disease (NAFLD), and cardiovascular disease [2]. Obesity is widely prevalent all over the world, with prevalence almost doubling since 1980 and with at least 2.8 million deaths per year due to obesity [3]. Adipose tissue is an energy storage site, which synthesizes and stores triglyceride (TG) to meet the needs of long-term energy storage [4]. It is also an endocrine organ, producing and secreting various adipokines including leptin, lipocalin, and interleukin-6, which is a major participant and regulator of obesity [5]. Pathological expansion of adipose tissue contributes to obesity [6], so targeted studies of adipocyte lipid metabolism have profound implications for the prevention and treatment of obesity.

Adipose tissue is mainly comprised of white adipose tissue (WAT) and brown adipose tissue (BAT). WAT accounts for about 90 % of the weight of fat and is the "energy pool". BAT mainly increases energy consumption through non-shivering thermogenesis, with a gradual age decline [7,8]. Beige adipose tissue, a newly defined adipose tissue, is produced by the browning of WAT, and its morphology and function are similar to BAT [9]. Upon activation by cold or β3-adrenergic agonists, WAT "browning" results in beige adipocytes that contain multi-chambered lipid droplets and abundant mitochondria, increasing thermogenesis and energy expenditure [10,11]. White fat browning promotes fat consumption and weight loss, which provides a new

[1]Institute of Digestive Disease, Guangxi Academy of Medical Sciences, The People's Hospital of Guangxi Zhuang Autonomous Region, Nanning, 530021, China [2]College of Animal Science and Technology, Guangxi University, Nanning, 530004, China [3]School of Pharmacy, Mongolian National University of Medical Sciences, Ulan Bator, 14200, Mongolia [4]Institute of Biomedical Science, Department of Histology, Mongolian National University of Medical Sciences, Ulan Bator, 14200, Mongolia

[5] These authors contributed equally to this work.

*Corresponding author. Institute of Digestive Disease, Guangxi Academy of Medical Sciences, The People's Hospital of Guangxi Zhuang Autonomous Region, Nanning City, Guangxi Zhuang Autonomous Region, 530021, China. E-mail: zhoulei@gxu.edu.cn (L. Zhou).

Received July 4, 2023 • Revision received January 1, 2024 • Accepted January 3, 2024 • Available online 9 January 2024

https://doi.org/10.1016/j.molmet.2024.101873

perspective and possible approach for treatment of obesity and its complications.

The mitochondrial calcium uniporter (*Mcu*) is a multimeric channel located in the inner membrane of mitochondria that facilitates Ca^{2+} transport to the mitochondrial matrix [12]. The *Mcu* multimeric channel is comprised of transmembrane subunits comprised of *Mcu*, *Mcub*, the essential *Mcu* regulatory protein (EMRE), and a membrane-gap heterodimer comprised of *Mcu*1 and *Mcu*2 [13]. Recently, a number of *Mcu* channel inhibitors have been identified including mitoxantrone (MTX), ruthenium red, and its derivative ruthenium 360 [14]. *Mcu*-mediated mitochondrial Ca^{2+} ($_mCa^{2+}$) transport plays a key role in maintenance of intracellular Ca^{2+} homeostasis and the regulation of cellular metabolism and apoptosis [15–17]. Specifically, the role of the *Mcu* in lipid metabolism has attracted more and more attention from researchers [18,19]. *Mcu* expression in adipose tissue demonstrated to increase during periods of obesity and diabetes [20]. Our previous study found that inhibition of hepatic *Mcu* prevented high-fat diet (HFD)-induced hepatic steatosis [21]. These studies identified a link between *Mcu*-mediated calcium transport and lipid metabolism, however the role of *Mcu* in adipose tissue remains to be further explored.

In this study, we assessed the effect of MTX, an inhibitor of *Mcu*, on mouse adipocyte lipid metabolism and found that MTX reduced adipocyte lipid accumulation. Further, adipose tissue-specific *Mcu* knockout mice were used to explore the effects of *Mcu* on obesity. Inhibition or depletion of *Mcu* resulted in resistance to diet-induced obesity with metabolic disorder improvements.

2. MATERIALS AND METHODS

2.1. Animals

C57BL/6J male mice were purchased from Guangxi Medical University (Nanning, China) and randomly divided into three groups (n = 6 per group) at 8 weeks of age: (1) ND group, fed normal diet (3.8 kcal/g) with intraperitoneal injection of saline. (2) HFD group, fed HFD (5.5 kcal/g) and intraperitoneal injection of saline. (3) HFD + MTX group, fed HFD and intraperitoneal injection of MTX (0.01 μM/kg body weight). The injection amount was 5 μL/g body weight, and the injection was given every 5 days for 12 weeks.

Mcu transgenic mice ($Mcu^{fl/fl}$) were purchased from Jackson Laboratory (Bar Harbor, ME, USA). Mice that expressed Cre recombinase under the control of the Adipoq promoter (Adipoq-Cre mice) were purchased from Cyagen Biosciences (Guangzhou, China). Adipose-specific heterozygous *Mcu* knockout ($Mcu^{fl/+}$ AKO) mice were generated by crossing $Mcu^{fl/fl}$ mice with Adipoq-Cre mice. $Mcu^{fl/fl}$ mice were used as controls. At 8 weeks of age, mice were divided into four groups (n = 6–9 per group): (1) $Mcu^{fl/fl}$ mice fed a normal diet ($Mcu^{fl/fl}$ ND), (2) $Mcu^{fl/+}$ AKO mice fed a normal diet ($Mcu^{fl/+}$ AKO ND), (3) $Mcu^{fl/fl}$ mice fed a high-fat diet ($Mcu^{fl/fl}$ HFD), and (4) $Mcu^{fl/+}$ AKO mice fed a high-fat diet ($Mcu^{fl/+}$ AKO HFD). Adipose-specific homozygous *Mcu* knockout ($Mcu^{fl/fl}$ AKO) mice were generated by crossing $Mcu^{fl/fl}$ mice with $Mcu^{fl/+}$ AKO mice. At the 8th week, the mice were divided into four groups (n = 9 per group) and fed standard chow or high-fat chow for 12 weeks.

Mice were free to feed and drink during the experiments and maintained under laboratory conditions (temperature range 23–26 °C, humidity range 40–70 %, 12 h light/dark cycle).

2.2. Ethics statement

All experimental protocols and procedures were approved by the Animal Experimentation Ethics Committee of Guangxi University (Gxu-2021-122).

2.3. Cell culture and differentiation

3T3-L1 cells was purchased from the ATCC (Manassas, VA, USA) and cultured in DMEM medium (Gibco, Beijing, China) containing 10 % fetal bovine serum (FBS) and 1 % antibiotics at 37 °C and 5 % CO_2. Two days after confluence (day 0), cells were induced for 2 days (day 2) in differentiation medium containing insulin (10 μg/mL), dexamethasone (1 μM), and 3-isobutyl-1-methylxanthine (0.5 mM) [22]. The medium was changed to DMEM medium containing insulin (10 μg/mL) for 2 days (day 4). During this process, the control group (MDI group) was treated without MTX (Selleck, Shanghai, China) and the experimental group (MDI + MTX group) was treated with 50 nM of MTX for 4 days. During differentiation, both groups were switched to DMEM medium containing 10 % FBS on day 5 and the medium was changed every 2 days for 8 days. The UN group was maintained in growth medium without inducing differentiation.

2.4. Western blot analysis

Briefly, approximately 20 μg of protein samples were subjected to sodium dodecyl sulfate-polyacrylamide gel electrophoresis, transferred to PVDF membranes, blocked with 5 % skim milk, and probed with primary antibody. Primary antibodies were obtained that reacted with: *Mcu* [Cell Signaling Technology, Danvers, MA, USA (CST); 14997S], PPARγ [Cell Signaling Technology, Danvers, MA, USA (CST); P37231], C/EBPα [Cell Signaling Technology, Danvers, MA, USA (CST); P49715], and tubulin [Beyotime, Shanghai, China; AF1216]. After incubation with goat anti-rabbit antibody or goat anti-mouse antibody, signals were detected with a Universal Hood II (BIO-RAD, Hercules, CA, USA).

2.5. Cell viability assay

3T3-L1 cells were seeded into 96-well plates and treated with different concentrations of MTX for 4 days. Cell viability was measured using a cell viability assay kit (Yeasen Biotechnology, Shanghai, China). Medium was removed from the wells and 10 μL of detection reagent was added to 90 μL of medium in each well for 1 h. Absorbance was measured with a microplate reader (Tecan M200 PRO; Männedorf, Switzerland) at 480 nm.

2.6. Triglyceride (TG) and total cholesterol (TC) measurement

TG and TC levels of cell and tissue samples were determined using a Tissue Cell Triglyceride Kit and a Tissue Cell Total Cholesterol Kit (Jiancheng Bioengineering Institute, Nanjing, China). All procedures were performed in strict accordance with the manufacturer's instructions.

2.7. Oil-red O staining

3T3-L1 cells were washed twice with PBS, fixed in 4 % paraformaldehyde, and stained with Oil Red O working solution for 30 min. The cells were photographed by fluorescence microscopy (Olympus U-RFL-T; Tokyo, Japan) after washing twice with PBS. Isopropanol was added to dissolve Oil Red O in lipid droplets and quantified with a microplate reader at a wavelength of 500 nm.

2.8. Measurement of cellular calcium levels

Mitochondrial (Mito), cytoplasmic (Cyto), and endoplasmic reticulum (ER) calcium contents were determined with 4 μM Rhod-2AM (MedChemExpress, Shanghai, China), 4 μM Fluo-4AM (Yeasen Biotechnology, Shanghai, China), and 5 μM Fluo-5N (ThermoFisher Scientific, Shanghai, China) fluorescent dyes. Cells were washed twice with Hank's balanced salt solution (HBSS) without Ca^{2+}, Mg^{2+}, stained by adding working dye solution, and incubated for 30 min at 37 °C. After washing twice, HBSS was added to each well and incubated for 20 min

at 37 °C. OD values were measured with a microplate reader (Tecan, Männedorf, Switzerland). Rhod-2AM, Fluo-4AM, and Fluo-5N were detected at 552nm/581 nm (Ex/Em), 494nm/516 nm (Ex/Em), and 494nm/516 nm (Ex/Em), respectively. The measured values were normalized to protein content.

2.9. Real-time quantitative PCR (qRT-PCR)

Total RNA was extracted using Trizol (Sigma-Aldrich, St Louis, MO, USA). After RNA concentration was determined, the RNA was reverse transcribed into cDNA. The 20 μL PCR reaction included 5 μL of cDNA, 10 μL of RealStar Green Fast Mixture (GenStar BioSolutions, Beijing, China), 1 μL of forward primer, 1 μL of reverse primer, and 3 μL of ddH_2O. qRT-PCR reactions were performed with a fluorescent quantitative gene amplifier (Analytik Jena, Germany). Primers that were used are listed in Supplementary Table 1.

2.10. Mitochondrial staining

Mitochondria were stained using Mito-Tracker Green (Beyotime, Shanghai, China) at a concentration of 100 nM. OD values at 490 nm/516 nm (Ex/Em) were measured using a microplate reader (Tecan, Männedorf, Switzerland).

2.11. Mitochondrial DNA analysis

Total DNA from 3T3-L1 cells was extracted using a prepared PCR lysis buffer. The relative amounts of mitochondrial DNA (mtDNA) and nuclear DNA were determined by qRT-PCR using primers listed in Supplementary Table 2, with the ratio between these two values reflecting the relative mitochondrial content.

2.12. Adenosine triphosphate (ATP) assay

Intracellular ATP was assayed using an ATP Assay Kit (Beyotime, Shanghai, China), with all procedures carried out in strict accordance with the kit instructions. A 100 μL volume of ATP assay working solution was added to each test well, followed by 20 μL of cell lysis supernatant. ATP levels were measured by a microplate reader (Tecan, Männedorf, Switzerland).

2.13. Genotype identification

Mouse tail DNA was extracted and PCR genotyping was performed using primers listed in Supplementary Table 3. The PCR products were separated by agarose gel electrophoresis and the gel was placed on a gel imaging system (Tocan, Shanghai, China) for photography.

2.14. Body composition analysis of mice

The body fat rate of mice was analyzed using the Niumag NMR analyzer (QMR23-060H-I; Suzhou, China). Put the standard into the instrument for calibration. After weighing the mouse, put it into the detection tube, enter the weight data of the mouse, and analyze the body fat data of the mouse.

2.15. Metabolic cages

After the mice had been acclimated to the system for 1 day, O_2 consumption, CO_2 production, respiratory exchange rate (RER), and energy expenditure were monitored using metabolic cages (Sable Systems International, North Las Vegas, Nevada, USA). During the experiment, mice were fed and watered *ad libitum*, using a 12 h/12 h light/dark cycle. With metabolic data, we used regression analyses of energy expenditure against body composition data [23,24]. We developed a linear model using body weight in relation to energy expenditure values, and subsequently brought in theoretical values of energy expenditure in the 40 g mice as a bias. This was used to correct for inaccuracies in energy expenditure data caused by differences in body weight.

2.16. Glucose tolerance and insulin sensitivity tests

For the glucose tolerance test (GTT), mice were injected intraperitoneally with a glucose solution (1.5 g/kg body weight) after 16 h of fasting [25]. Blood glucose levels were measured at 0, 15, 30, 60, 90, and 120 min. For the insulin sensitivity test (ITT), mice were injected intraperitoneally with insulin (1 unit/kg of body weight) after 4 h of fasting. Blood glucose levels were measured at 0, 15, 30, 60, 90, and 120 min [26].

2.17. Micro-computed tomography (micro-CT) analysis

Mice were anaesthetized by intraperitoneal injection of tribromoethanol (TCI; Shanghai China), placed supine in a scanning chamber, and analyzed for fat distribution by micro-computed tomography (Bruke SkyScan 1278; Bielerica, Massachusetts, USA) [27]. Scan results were acquired with reconstruction software (NRECON) and analysis software (Dataviewer, CTVOX, CTAN) [28].

2.18. RNA-seq

Total RNA was isolated by standard TRIzol protocol. A total amount of 1−3 μg RNA per sample was prepared for subsequent library construction and high-throughput sequencing. RNA libraries were prepared according to the protocol of the VAHTS Universal V6 RNA-seq Library Prep Kit for Illumina ® (NR604-01/02) following the manufacturer's recommendations (Annoroad Gene Technology Co. Ltd., Beijing, China). And the raw sequencing reads were generated on an illumina nova x plus.

2.19. Statistical analysis

All experiments were performed at least three times independently. All data are expressed as the means ± SEM. Statistical analysis was performed using unpaired two-tailed t-tests (two groups) or ANOVA (multiple groups). Differences were considered statistically significant if $P < 0.05$ (*) or $P < 0.01$ (**).

3. RESULTS

3.1. Inhibition of *Mcu* reduces adipocyte differentiation and lipid accumulation

To investigate the role of the *Mcu* in adipocyte lipid accumulation, we first examined *Mcu* expression before and after adipocyte differentiation. Interestingly, *Mcu* expression was found to increase following 3T3-L1 cells differentiation (Figure 1A), indicating a positive relationship between *Mcu* expression and adipocyte differentiation. Therefore, we hypothesized that inhibition of *Mcu* channels may reduce adipocyte differentiation. We chose a known inhibitor of *Mcu*, mitoxantrone (MTX), to test this conjecture. MTX at a concentration of 100 nM did not affect 3T3-L1 cells activity (Figure 1B). As an inhibitor of *Mcu* channels, MTX significantly decreased the amount of $_{m}Ca^{2+}$ (Figure 1C), increased Ca^{2+} within the ER (Figure 1D), with no change in the content of Ca^{2+} within the Cyto (Figure 1E). 3T3-L1 cells were cultured in differentiation medium +50 nM mitoxantrone (MDI + MTX group) or in differentiation medium without MTX (MDI group) for 4 days (Figure 1F). Intracellular TG levels were reduced with 50 nM MTX (Figure 1G). This result was confirmed by Oil Red O staining, with fewer red lipid droplets within MTX-treated cells (Figure 1H). CCAAT/enhancer-binding protein alpha (C/EBPα) and peroxisome proliferator-activated receptor gamma (PPARγ) are early

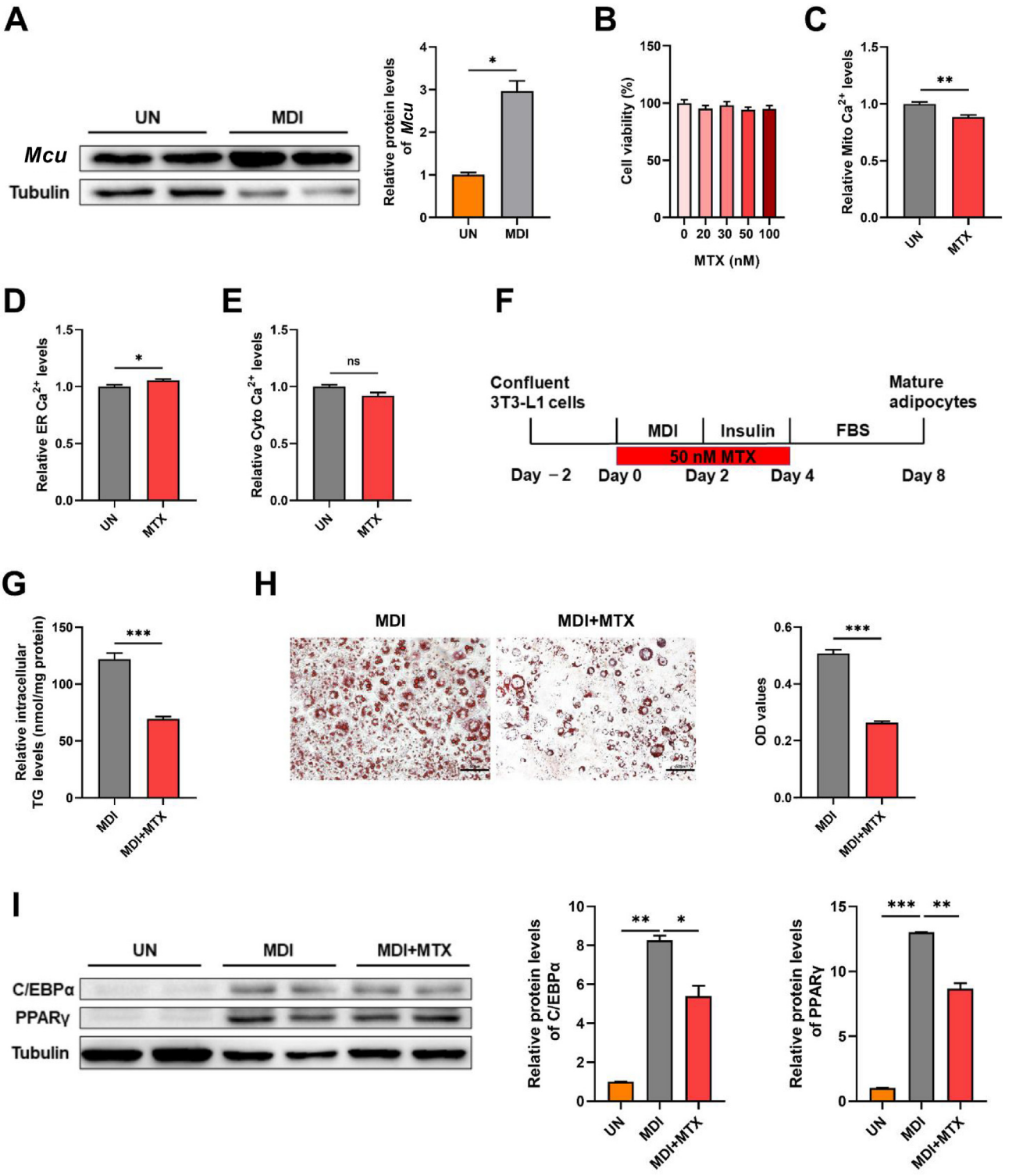

Figure 1: Inhibition of *Mcu* reduces adipocyte differentiation and lipid accumulation. (A) The levels of *Mcu* protein in mouse adipocytes (3T3-L1 cells) before differentiation (UN) and after differentiation (MDI). (B) Viability assay of 3T3-L1 cells after 4 d of MTX treatment (n = 6). (C) Relative mitochondrial calcium levels before and after MTX treatment in un-induced 3T3-L1 cells (n = 3). (D) Relative endoplasmic reticulum calcium levels (n = 3). (E) Relative cytoplasmic calcium levels (n = 3). (F) Schematic diagram of MTX treatment of 3T3-L1 cells. UN group: maintained in growth medium without differentiation; MTX group: maintained in growth medium with MTX for four days; MDI group: normal induction of differentiation for 8 days; MDI + MTX group: additional 50 nM MTX added during day 0 − day 4 of differentiation. (G) Intracellular triglyceride (TG) levels (n = 4). (H) Oil red O staining of 3T3-L1 cells and absorbance values at 500 nm. Scale bar, 50 μm (n = 4). (I) Western blot measurement of C/EBPα and PPARγ protein levels. Data are represented as means ± SEM. $*p < 0.05$, $**p < 0.01$, $***p < 0.001$.

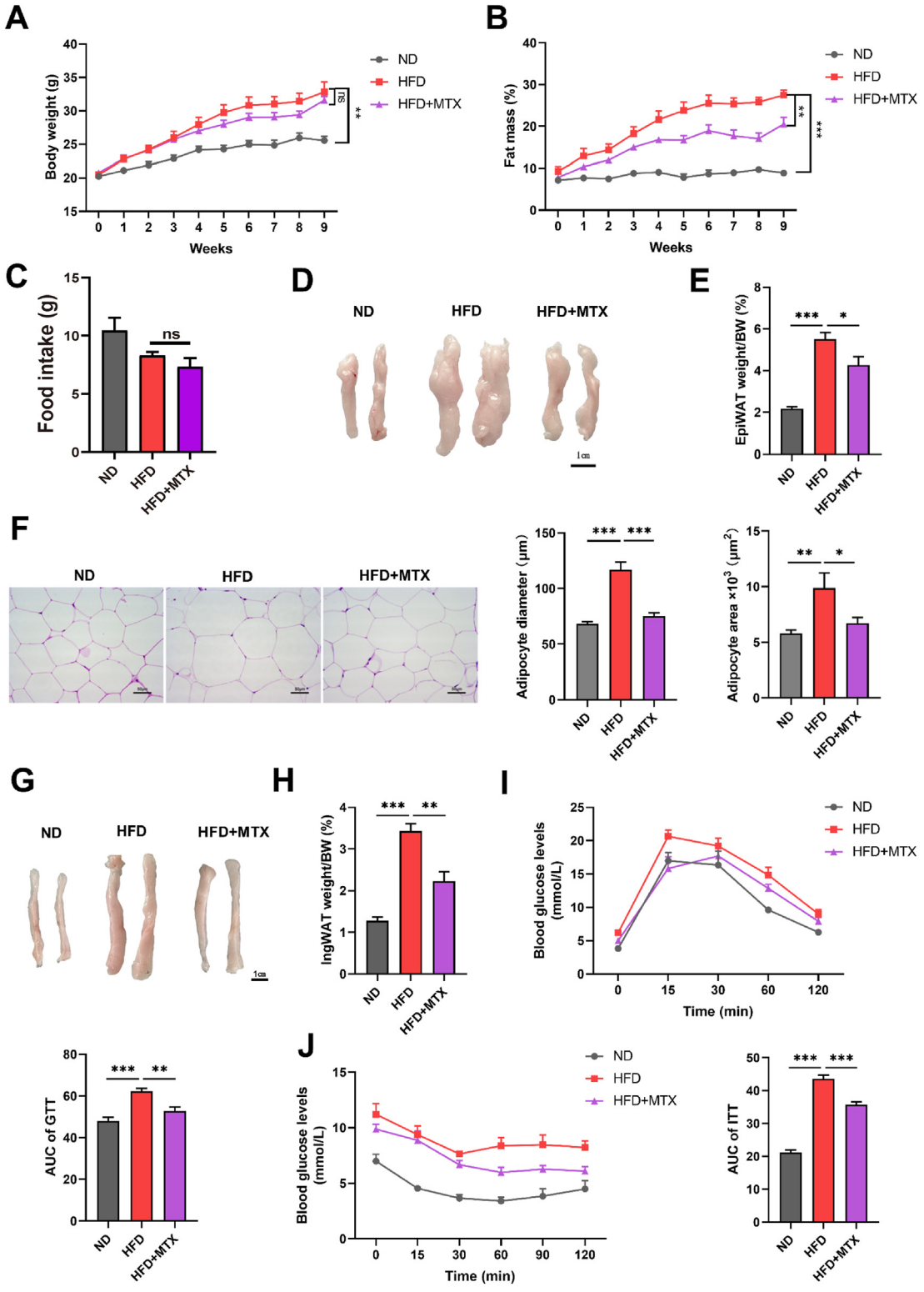

Figure 2: Inhibition of *Mcu* alleviates obesity and metabolic disorders induced by a high-fat diet (A) Body weight of mice (n = 6). (B) Body fat ratio of mice (n = 6). (C) Food intake of mice over four days (n = 4). (D) Representative photograph of adipose tissue of mouse epididymis (EpiWAT). (E) Ratio of EpiWAT weight/body weight of mice (n = 5). (F) H&E staining of mouse EpiWAT and quantification of cell diameter and area. Scale bar, 50 μm. (G) Representative photographs of mouse inguinal adipose tissue (iWAT). (H) Ratio of iWAT weight/body weight in mice (n = 5). (I) Glucose tolerance and quantification of area under curve (AUC) analysis of mice (n = 6). (J) Insulin sensitivity and quantification of the AUC of mice (n = 6). Data are represented as means ± SEM. $*p < 0.05$, $**p < 0.01$, $***p < 0.001$.

markers of adipocyte differentiation [29,30]. MTX decreased the expression of C/EBPα and PPARγ (Figure 1I). Taken together, these results suggest that *Mcu* inhibits differentiation of 3T3-L1 cells and reduces adipocyte lipid deposition by regulation of mitochondrial calcium homeostasis.

3.2. Inhibition of *Mcu* alleviates obesity and metabolic disorders induced by a high-fat diet

We next examined the effect of MTX on obesity and related metabolic disorders in mice. Eight-week-old mice were divided into three groups: normal diet group (ND group), high fat diet group (HFD group), and high fat diet + mitoxantrone group (HFD + MTX group). The HFD + MTX group was injected with MTX (0.01 μM/kg body weight) intraperitoneally. Compared with the HFD group, MTX reduced the body weight of mice without statistically significant difference ($P = 0.47$; Figure 2A) and significantly reduced body fat (Figure 2B). There was no significant difference in food intake between the HFD and HFD + MTX groups (Figure 2C). MTX treatment alleviated HFD-induced epididymal fat expansion (Figure 2D-E). H&E staining showed a significant reduction in adipocyte size and diameter in the MTX-treated group compared to the HFD group (Figure 2F). Similarly, MTX treatment significantly reduced inguinal fat (Figure 2G-H). Further, MTX improved HFD-induced glucose intolerance and insulin resistance (Figure 2I-J). These results suggest that MTX reduced HFD-induced fat accumulation and that *Mcu* plays a key role in obesity resistance and metabolic disorder improvements.

3.3. *Mcu* knockdown within adipose tissue alleviates high-fat diet-induced metabolic disorders

To explore the mechanism of action of MTX, we bred heterozygous adipose tissue-specific *Mcu* knockdown mice ($Mcu^{fl/+}$ AKO) to simulate adipose tissue *Mcu* inhibition by crossing $Mcu^{fl/fl}$ mice with Adipoq-Cre mice (Figure 3A). Genotype identification confirmed mice genotypes (Figure 3B). Expression of *Mcu* in epididymal fat (EpiWAT), inguinal fat (iWAT), and BAT was reduced in $Mcu^{fl/+}$ AKO mice (Figure 3C). Expression was unchanged in the heart, liver, and kidney, which confirmed the specific knockdown of *Mcu* in adipose tissue (Figure 3D). Eight-week-old $Mcu^{fl/fl}$ mice and $Mcu^{fl/+}$ AKO mice were fed a normal diet (ND) or a high-fat diet (HFD). There was no significant difference in body weight between $Mcu^{fl/fl}$ mice and $Mcu^{fl/+}$ AKO mice (Figure 3E), and there was no significant difference in food intake (Figure S2A). However, with HFD conditions, the body fat of $Mcu^{fl/+}$ AKO mice was decreased significantly compared to $Mcu^{fl/fl}$ mice (Figure 3F-G). The distribution of adipose tissue in the mice was visualized by Micro-CT scanning and the results showed a significant reduction in body fat accumulation in $Mcu^{fl/+}$ AKO mice (Figure 3H). The weight of EpiWAT was significantly reduced in the $Mcu^{fl/+}$ AKO HFD group, but no significant change in Ing WAT weight (Figure 3I-J), with a slight increase in the weight of BAT that was not significant ($P = 0.211$, Figure 3K-L). Further, mice in the $Mcu^{fl/+}$ AKO HFD group showed better glucose tolerance than the $Mcu^{fl/fl}$ HFD group (Figure 3M). Energy metabolism analysis of mice for both ND and HFD conditions found that $Mcu^{fl/+}$ AKO mice had greater O_2 consumption and CO_2 production than the control group, with no significant difference in RER (Figs. S1A—C). After measuring the energy expenditure of mice in the ND and HFD groups (Figs. S1D—E), we observed a significant increase in the energy expenditure of mice in the $Mcu^{fl/fl}$ AKO HFD compared to that of the $Mcu^{fl/+}$ HFD group (Fig. S1E). Thermographic analysis of mice at room temperature found that $Mcu^{fl/+}$ AKO mice had a significantly higher body surface hyperthermia than control mice (Fig. S1F), indicating that knockdown of adipose tissue *Mcu* increased heat production. These results suggest that knockdown of *Mcu* in adipose tissue alleviates HFD-induced obesity and improves metabolic disorders in mice. This effect may be caused by increased aerobic respiration and enhanced energy expenditure.

3.4. Adipose tissue specific knockout of *Mcu* improves obesity and health status induced by a high-fat diet

To investigate the effect of *Mcu* on fat deposition, we bred homozygous $Mcu^{fl/fl}$ AKO mice. *Mcu* was not expressed in adipose tissue of $Mcu^{fl/fl}$ AKO mice, but did not change in the heart, liver, and kidney (Figure 4A-B). In the HFD groups, mice lacking *Mcu* showed significantly lower body weight gains than controls, with no effect on ND mice (Figure 4C). We also found that $Mcu^{fl/fl}$ AKO HFD mice were slimmer and had significantly lower body fat compared to the $Mcu^{fl/fl}$ HFD group (Figure 4D-E), and there was no significant difference in food intake (Figure S2B). Similarly, Micro-CT scans showed less fat in $Mcu^{fl/fl}$ AKO mice (Figure 4F). Further, EpiWAT and iWAT were decreased, BAT was unchanged, but BAT color was redder in $Mcu^{fl/fl}$ AKO mice compared to controls (Figure 4G-H). H&E staining showed a significant reduction in the size of individual adipocytes within EpiWAT, iWAT, and BAT of $Mcu^{fl/fl}$ AKO mice (Figure 4I-J). These results suggest that the absence of *Mcu* in adipose tissue reduces the expansion of adipose tissue and alleviates HFD-induced obesity.

Given that health problems such as hepatic steatosis, dyslipidemia, and insulin resistance are closely associated with obesity [31], we assessed the effect of adipose *Mcu* deficiency on the health status of mice. $Mcu^{fl/fl}$ HFD mice exhibited hepatic lipid accumulation as evidenced by increased liver volume and weight, yellowing in color, with H&E and Oil Red O staining demonstrating aggregation of lipid droplets in the liver. $Mcu^{fl/fl}$ AKO HFD mice exhibited a significant reduction in liver weight and lipid accumulation (Figure 5A-B). Further, liver TG and TC levels in $Mcu^{fl/fl}$ AKO HFD mice were significantly lower than those of the control group (Figure 5C). Under HFD conditions, $Mcu^{fl/fl}$ AKO mice exhibited reduced serum levels of aspartate aminotransferase (AST) and alanine aminotransferase (ALT), indicating that *Mcu* deficiency alleviated liver damage (Figure 5D). Moreover, serum lipid levels, including TG, TC, and low-density lipoprotein (LDL) were significantly reduced. High-density lipoprotein (HDL) levels were increased (Figure 5E). The decrease in circulating lipid levels may partially explain the resistance of $Mcu^{fl/fl}$ AKO mice to obesity. Obesity is often accompanied by abnormal glucose metabolism and insulin resistance [32]. $Mcu^{fl/fl}$ AKO HFD mice had significantly lower fasted blood glucose than mice of the $Mcu^{fl/fl}$ HFD group (Figure 5F). $Mcu^{fl/fl}$ AKO HFD mice exhibited better glucose tolerance and insulin sensitivity compared to the $Mcu^{fl/fl}$ HFD group (Figure 5G-H). These results suggest that adipose tissue *Mcu* deficiency alleviates hepatic steatosis, decreases blood lipid levels, reduces insulin resistance, and improves health under HFD conditions.

3.5. Adipose tissue-specific knockout of *Mcu* increases energy expenditure and thermogenesis

To explore the *Mcu* mechanism of action, we monitored energy metabolism and heat production in mice. Compared with the $Mcu^{fl/fl}$ HFD group, O_2 consumption and CO_2 production were significantly increased in $Mcu^{fl/fl}$ AKO HFD mice (Figure 6A-B), with no significant difference in RER (Figure 6C). Measuring the energy expenditure of mice in the ND and HFD groups (Figure 6D-E), we found that the energy expenditure of mice in the $Mcu^{fl/fl}$ AKO HFD group was significantly higher than that of the $Mcu^{fl/fl}$ HFD group (Figure 6E,Figure S3 A-B). These results imply that adipose tissue *Mcu* deficiency may increase aerobic respiration and basal metabolic activity. Thermographic analysis of mice at room

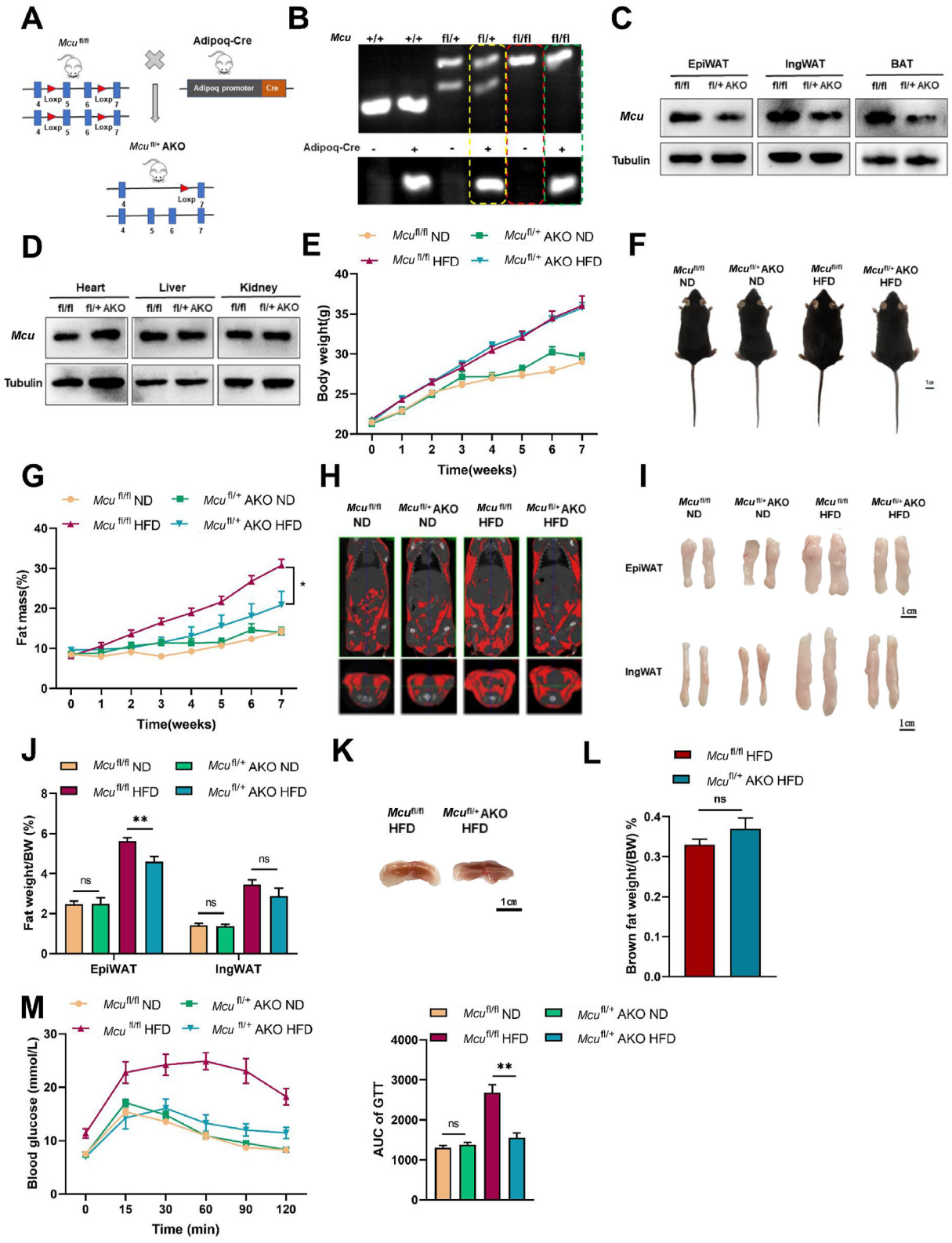

Figure 3: *Mcu* knockdown of adipose tissue alleviates high-fat diet-induced metabolic disorders. (A) Schematic diagram of adipose-specific heterozygous *Mcu* knockdown generation. (B) Mouse PCR genotype identification (yellow boxes indicates the *Mcu* $^{fl/+}$ AKO mouse genotype, red boxes indicate the *Mcu*$^{fl/fl}$ mouse genotype, green boxes indicate the *Mcu*$^{fl/fl}$ AKO mouse genotype). (C) Western blot of *Mcu* in adipose tissue. (D) Western blot of *Mcu* in heart, liver, and kidney. (E) Body weight of mice (n = 6–9). (F) Typical photographs of mouse body size at the end of the experiment. (G) Body fat ratio in mice (n = 6–9). (H) CT imaging of mice. (I) Typical photographs of EpiWAT and iWAT in mice. (J) EpiWAT weight/body weight ratio, iWAT weight/body weight ratio (n = 6). (K) Typical photographs of brown adipose tissue (BAT) with a high-fat diet. (L) BAT weight/body weight ratio (n = 6). (M) Glucose tolerance analysis of mice and quantification of AUC (n = 4–9). Data are represented as means ± SEM. $*p < 0.05$, $**p < 0.01$, $***p < 0.001$.

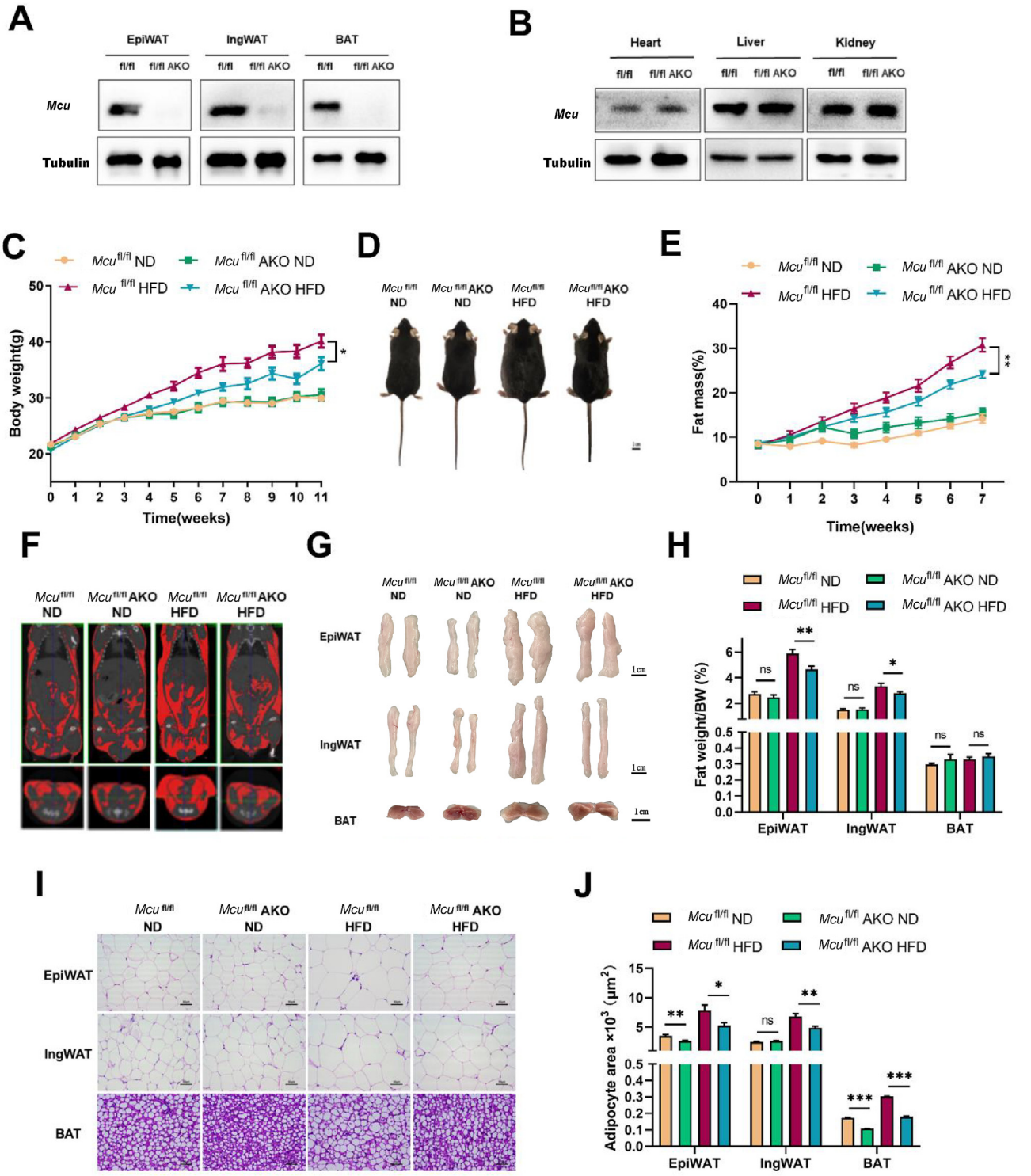

Figure 4: Adipose tissue specific knockout of *Mcu* ameliorates high-fat diet-induced fat deposition. (A) Western blot of *Mcu* in adipose tissue. (B) Western blot of *Mcu* in other tissues. (C) Mouse body weight (n = 8–9). (D) Typical photographs of mouse body size at the end of the experiment. (E) Mouse body fat ratio (n = 8–9). (F) CT imaging of mice. (G) Typical photographs of EpiWAT, iWAT, and BAT in mice. (H) Weight/body weight of EpiWAT, iWAT, and BAT (n = 6–9). (I) H&E staining of mouse adipose tissue. Scale bar, 50 μm. (J) Adipocyte size. Data are represented as means ± SEM. $^{*}p < 0.05$, $^{**}p < 0.01$, $^{***}p < 0.001$.

temperature found that *Mcu*$^{fl/fl}$ AKO HFD mice had more high temperature body surface areas than *Mcu*$^{fl/fl}$ HFD mice (Figure 6F). Meanwhile, we performed RNA-seq of adipose tissue from *Mcu*$^{fl/fl}$ HFD mice and *Mcu*$^{fl/fl}$ AKO HFD mice, and found that thermogenesis-related genes were affected in *Mcu*$^{fl/fl}$ AKO HFD mice (Supplementary Table S4). These results suggest that under HFD conditions *Mcu*$^{fl/fl}$ AKO mice resist obesity by promotion of energy expenditure, increasing thermogenesis, and thus reducing body fat deposition.

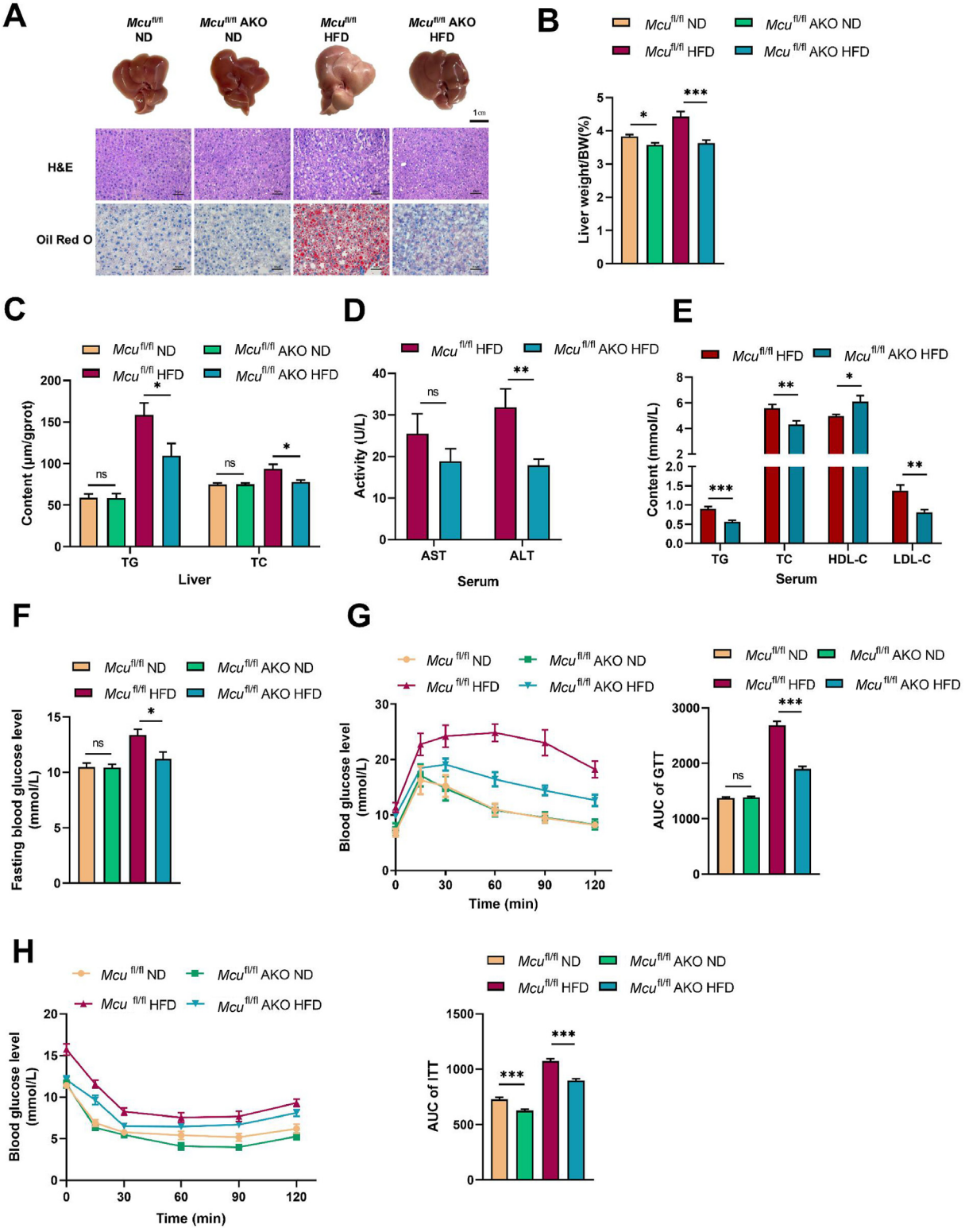

Figure 5: Adipose tissue specific knockout of *Mcu* improves health in high-fat diet-induced mice. (A) Typical photographs of mouse liver, mouse liver H&E staining, and mouse liver Oil Red O staining. Scale bar, 50 μm. (B) Mouse liver weight/body weight ratio (n = 9). (C) Mouse liver TG and total cholesterol (TC) levels (n = 6–9). (D) Serum aspartate aminotransferase (AST) and alanine aminotransferase (ALT) activities in mice with a high-fat diet (n = 6–7). (E) Serum TG, TC, high-density lipoprotein, cholesterol (HDL-C), and low-density lipoprotein cholesterol (LDL-C) levels in mice with a high-fat diet (n = 7). (F) Blood glucose levels in fasting mice (n = 6–8). (G) Glucose tolerance and quantification of AUC analysis of mice (n = 7–9). (H) Insulin sensitivity of mice and quantification of AUC (n = 9). Data are represented as means ± SEM. $*p < 0.05$, $**p < 0.01$, $***p < 0.001$.

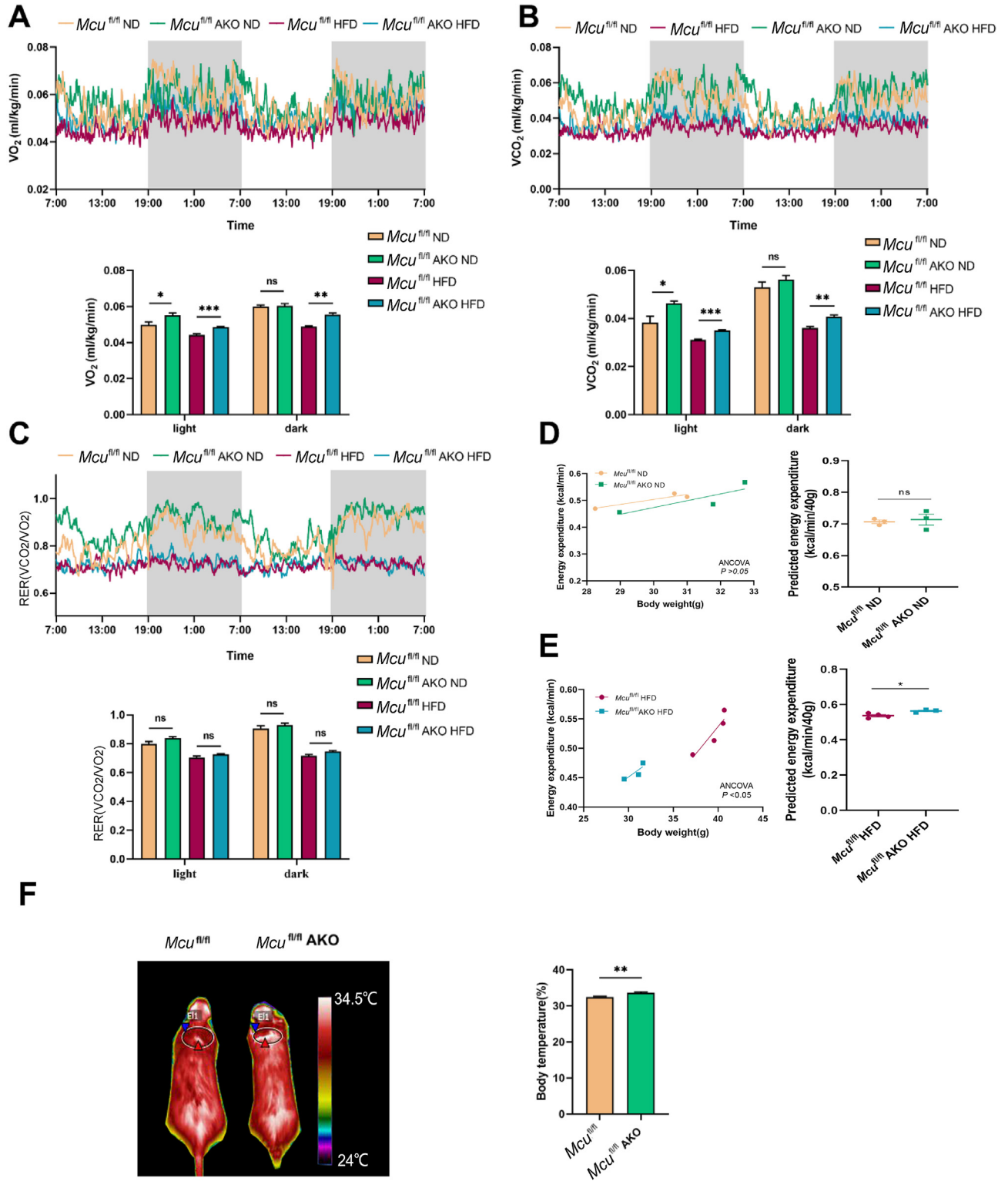

Figure 6: Adipose tissue-specific knockout of *Mcu* increases energy expenditure and thermogenesis. (A) O_2 consumption in mice during the experiment (n = 3–4). (B) CO_2 production (n = 3–4). (C) Respiratory exchange rate (RER) (n = 3–4). (D) *Mcu*$^{fl/fl}$ ND and *Mcu*$^{fl/fl}$ AKO ND were assessed by ANCOVA (analysis of covariance) (n = 3). (E) *Mcu*$^{fl/fl}$ HFD and *Mcu*$^{fl/fl}$ AKO HFD were assessed by ANCOVA (analysis of covariance) (n = 3–4). (F) Body temperature of *Mcu*$^{fl/fl}$ HFD mice and *Mcu*$^{fl/fl}$ HFD AKO mice at room temperature (n = 4–5). Data are represented as means ± SEM. *$p < 0.05$, **$p < 0.01$, ***$p < 0.001$.

3.6. Inhibition of *Mcu* promotes mitochondrial biogenesis and activates adipocyte browning

Excessive $_{m}Ca^{2+}$ levels can cause mitochondrial dysfunction [33]. By comparing $_{m}Ca^{2+}$ levels before and after adipocyte differentiation, $_{m}Ca^{2+}$ levels were found to be significantly upregulated after adipocyte differentiation, which was reversed after MTX treatment (Figure 7A). Adipocyte differentiation resulted in a significant decrease in mtDNA copy number, with MTX treatment increasing the number of mitochondria (Figure 7B). Results of mitochondrial staining were consistent, indicating that the number of mitochondria decreased after adipocyte differentiation and increased with MTX treatment (Figure 7C). Lipid peroxidation occurs when the dynamic balance between the oxygen radical response and lipid peroxidation is disturbed, which can contribute to mitochondrial damage [34]. Adipocyte differentiation resulted in a significant increase in ROS levels, while MTX treatment reduced intracellular ROS levels (Figure 7D). Superoxide dismutase (SOD), an important antioxidant enzyme, was significantly increased in the MDI + MTX group compared to the MDI group (Figure 7E). In addition, we found that MTX treatment increased intracellular ATP (Figure 7F). Mitochondrial membrane potential (MMP), which reflects mitochondrial viability, was increased by MTX treatment (Figure 7G). These results suggest that MTX promotes mitochondrial biogenesis and enhances mitochondrial activity. Subsequently, we examined the expression of white fat browning marker genes. The mRNA expression levels of uncoupling protein 1 (*UCP1*), peroxisome proliferator-activated receptor γ coactivator 1α (*PGC-1*α), PR-domain-containing 16 (*PRDM16*), and pyruvate dehydrogenase kinase 4 (*PDK4*) were significantly increased in the MDI + MTX group compared to the MDI group (Figure 7H). Moreover, to determine whether MTX affects lipid metabolism in mature adipocytes, we treated differentiated 3T3-L1 cells with MTX for 4 days and found that MTX treatment reduced $_{m}Ca^{2+}$ content and cellular lipid levels (Figure 7I-J). Oil Red O staining showed similar results (Figure 7K). These results demonstrate that inhibition of *Mcu* channels not only inhibits adipocyte differentiation but also reduces fat deposition in mature adipocytes. Further, MTX treatment produces a beneficial maintenance of mitochondrial function and promotes browning of white adipocytes by inhibition of *Mcu*-mediated calcium transport.

4. DISCUSSION

In this study, we found that MTX, an *Mcu* channel inhibitor, reduced lipogenic differentiation and fat deposition in 3T3-L1 cells. *In vivo* experiments showed that MTX alleviated HFD-induced obesity and insulin resistance. By constructing *Mcu* adipose tissue-specific knockout mice, adipose tissue *Mcu* deletion was shown to increase resistance to obesity and to enhance energy consumption of mice fed a HFD. Mechanistic studies demonstrated that inhibition of adipose tissue *Mcu* downregulates $_{m}Ca^{2+}$ overload, enhances mitochondrial biosynthesis, enhances mitochondrial activity, and promotes browning of white adipocytes. These results provide a new perspective for the treatment of obesity.

As a multifunctional signaling molecule, calcium is required for a number of biological processes, including cell proliferation, differentiation, and apoptosis [35–37]. Further, lipid accumulation in adipocytes is strongly influenced by intracellular Ca^{2+} homeostasis. Wang et al. showed that Cisd2 deletion increased adipocyte Ca^{2+} levels and induced calcineurin signaling, thereby inhibiting adipogenesis [38]. However, we found that MTX reduced $_{m}Ca^{2+}$ levels in adipocytes, but did not affect intracellular calcium content (Figure 1C-E), suggesting that MTX regulates $_{m}Ca^{2+}$ overload by inhibiting Ca^{2+} influx from the endoplasmic reticulum (ER) rather than altering cytoplasmic Ca^{2+} content. Calcium stored in the ER can be transferred to the mitochondria through *Mcu* transmission as required [39]. When a small amount of calcium enters the mitochondria, it activates the tricarboxylic acid cycle to increase ATP production and facilitate metabolic homeostasis [40,41]. While $_{m}Ca^{2+}$ overload triggers mitochondrial dysfunction and leads to apoptosis [42]. We found that $_{m}Ca^{2+}$ levels were significantly upregulated after adipocyte differentiation and that lowering $_{m}Ca^{2+}$ levels inhibited adipocyte differentiation and reduced cellular lipid accumulation (Figure 7A, Figure 1G-I). Similarly, Ding et al. found that supplementation with $_{m}Ca^{2+}$ promoted lipid storage in seipin mutant adipocytes [43]. Based on these findings, it appears that $_{m}Ca^{2+}$ homeostasis is essential for adipogenic differentiation, suggesting that alleviating $_{m}Ca^{2+}$ overload would reduce lipid accumulation in adipocytes.

The *Mcu*, as a key ion channel for $_{m}Ca^{2+}$ transport, has been shown to regulate a variety of cell biological processes. Increased *Mcu* expression has been observed in insulin-resistant adipocytes [20]. This study found that the level of *Mcu* expression increased after adipocyte differentiation (Figure 1A). Gao et al. showed that SIRT3 inhibited aging-induced BAT whitening by suppressing *Mcu*-mediated $_{m}Ca^{2+}$ overload [44]. Xue et al. found that the *Mcu*-EMRE-UCP1 complex in brown adipose tissue could serve as a target for obesity prevention [45]. These studies suggest that *Mcu* plays an important role in regulating adipocyte metabolism. The function of *Mcu* has been studied using a wide range of conditional knockout mice, and we recently discovered that liver-specific *Mcu* knockout mice were resistant to NAFLD induced by HFD [21]. Flicker et al. found that deletion of *Mcu* in BAT had no significant effect on diet-induced obesity in mice [46]. Herein, we observed similar results in both $Mcu^{fl/+}$ AKO mice and $Mcu^{fl/fl}$ AKO mice, in which a reduction in fat was found with HFD conditions (Figure 3G, Figure 4E). And by performing RNA-seq on iWAT and BAT, we found that some thermogenic genes were altered in AKO mice. The detected thermogenic genes included Ucp1-dependent gene (*Ucp1, Prdm16, Ehmt1*); calcium cycle gene (*Sln*); creatine cycle gene (*Ckb, Alpl, Gatm*); lipid cycle gene (*Atf4, Cd36, Cebpb, Cidea, Fabp4, Pparg, Ppargc1a*); Ucp1-independent mitochondrial uncoupling gene (*Slc25a4, Slc25a5*) (Table S4). Among them, we found a significant increase in *Ucp1* expression in iWAT and an insignificant change in BAT. We believe this is similar with Flicker's results that *Mcu* has no effect on BAT's thermogenesis. Kozak et al. showed that Ucp1 deficiency does not alter energy expenditure in adipose tissue, but relies on thermogenesis that enhances ion and substrate cycling capacity [47]. However, our findings indicated that *Mcu* deletion upregulates Ucp1 expression in iWAT (Table S4) and 3T3L-1 cells (Figure 7H), and may increase energy expenditure by promoting thermogenesis. It is an interesting result, suggesting that *Mcu* play a role in iWAT. We believe that the regulatory mechanism of *Mcu* on Ucp1 expression in iWAT is a question that deserves further investigation.

Mitochondria are the center of cellular energy metabolism and an important hub for cell signaling, with involvement in a wide range of physiological activities [48,49]. During cardiac ischemia/reperfusion, inhibition of *Mcu* function facilitates the balance of mitochondrial autophagy and fusion and reduces structural damage to mitochondria [50]. We also found that inhibition of *Mcu* channels facilitated mitochondrial biogenesis, increasing cellular ATP levels, and enhancing mitochondrial number (Figure 7F, B-C). Prolonged $_{m}Ca^{2+}$ overload results in increased intracellular ROS and open mPTP, resulting in mitochondrial damage and induction of cell death [51]. Liao et al. found that inhibition of *Mcu* activity induced cellular resistance to oxidative

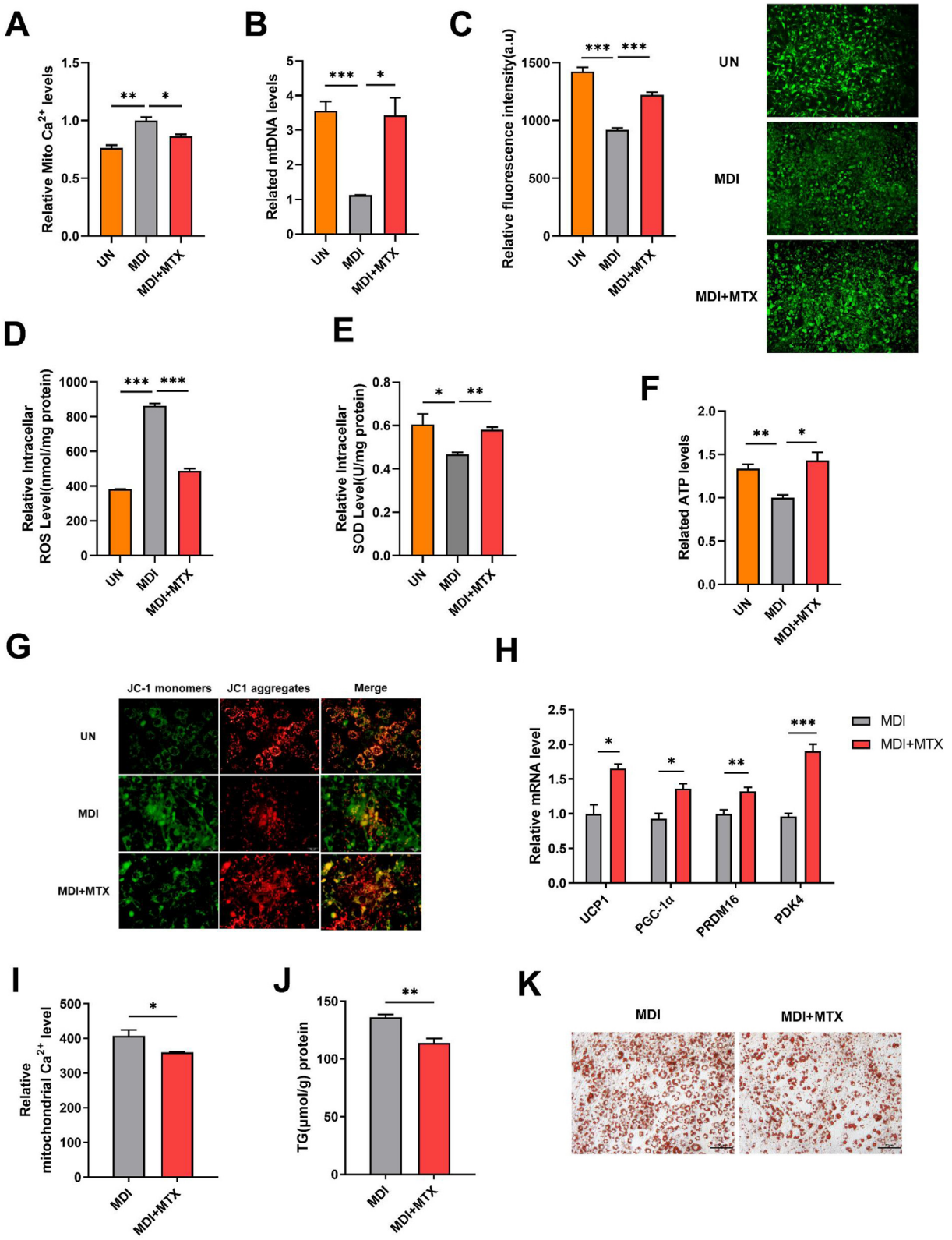

Figure 7: Inhibition of *Mcu* promotes mitochondrial biogenesis and activates adipocyte browning. (A) Mitochondrial calcium levels in un-induced 3T3-L1 cells (UN), induced differentiation (MDI), and treatment with 50 nM MTX for 4 days during induced differentiation (MDI + MTX) (n = 3). (B) Copy number of mitochondrial DNA (mtDNA) in 3T3-L1 cells with 18sRNA as an internal reference (n = 3). (C) Mitochondrial fluorescence staining of 3T3-L1 cells and their fluorescence intensity (n = 3). (D) 3T3-L1 cells reactive oxygen species (ROS) levels (n = 3). (E) Cellular superoxide dismutase (SOD) levels (n = 3). (F) Cellular adenosine triphosphate (ATP) levels (n = 3). (G) Mitochondrial membrane potential (MMP) assay. (H) Cellular browning-related genes (*UCP1*, *PGC-1α*, *PRDM16*, and *PDK4*) mRNA expression levels (n = 3–4). (I) After cell differentiation 8 days without MTX treatment (MDI) and 4 days of treatment with MTX (MDI + MTX). Mitochondrial calcium level measurement (n = 3). (J) Intracellular TG content (n = 3). (K) Oil Red O staining of cells. Data are represented as means ± SEM. $^{*}p < 0.05$, $^{**}p < 0.01$, $^{***}p < 0.001$.

stress [52]. Consistent with those results, this study found that MTX restored $_{m}Ca^{2+}$ levels and reduced intracellular ROS levels, increased SOD activity, and alleviated cellular oxidative stress (Figure 7D-E). An increase in the number of mitochondria is a distinctive feature of white fat browning. Genes such as *Ucp1*, *Pgc-1α*, *Prdm16*, and *Pdk4* are widely used as precursor markers for white fat browning [53,54]. In this study, MTX significantly upregulated the mRNA expression levels of these genes (Figure 7H). Thermography also showed that *Mcu* knockout increased thermogenesis in mice. Overall, these results suggest that inhibition of *Mcu* increases mitochondrial activity and promotes adipocyte browning.

In summary, these results suggest that regulation of $_{m}Ca^{2+}$ levels is a key process affecting adipocyte differentiation and that reductions in adipocyte $_{m}Ca^{2+}$ levels decrease intracellular lipid accumulation. Adipose-specific *Mcu* deficiency alleviates HFD-induced obesity and ameliorates metabolic disorders such as insulin resistance and hepatic steatosis. These effects may be achieved by increasing mitochondrial biosynthesis, promoting white fat browning, and enhancing energy metabolism. Further, this study demonstrated a link between adipocyte lipid accumulation and $_{m}Ca^{2+}$ levels, suggesting that *Mcu* is a potential therapeutic target for treatment of obesity and obesity-related metabolic diseases.

Finally, this study has potential limitations. The first limitation is food intake, in our study food intake was recorded with a period of $=4$ days. Although there was no significant difference in food intake between groups in this study, if food intake can be detected for a longer period of time, it will be able to determine the effect of food intake on body weight more accurately. The second limitation is the sample size. We believe that if the sample size can be further increased, it will help to get more accurate results. The last limitation is the experimental method of GTT, the reference method used in this study being an injection of 1.5 g/kg glucose in mice [25], followed by measurement of plasma glucose levels. Other studies have shown that administering a fixed dose of glucose in mice can also be used to measure GTT [55]. In future studies, we can try multiple GTT methods in order to get more accurate results.

AUTHOR CONTRIBUTIONS

Mengting Jia: Writing — review & editing, Writing — original draft, Visualization, Validation, Software, Methodology, Investigation, Data curation, Conceptualization. **Siqi Liu:** Writing — review & editing, Visualization, Validation, Software, Methodology, Formal analysis, Data curation, Conceptualization. **Yang Xiao:** Writing — review & editing, Validation, Software, Resources, Methodology. **Zhiwang Zhang:** Writing — review & editing, Visualization, Methodology, Investigation, Formal analysis. **Mingming Li:** Writing — review & editing, Software, Methodology, Investigation. **Xinyu Qi:** Writing — review & editing, Software, Methodology, Formal analysis. **Xinyi Qi:** Writing — review & editing, Visualization, Methodology, Investigation. **Lin Yu:** Writing — review & editing, Formal analysis, Conceptualization. **Caiyong Zhang:** Writing — review & editing, Visualization, Software. **Tianyu Jiang:** Writing — review & editing, Methodology, Investigation. **Tingli Pan:** Writing — review & editing, Methodology, Investigation. **Yu Sun:** Writing — review & editing, Methodology, Investigation. **Jingsu Yu:** Writing — review & editing, Software. **Songtao Su:** Writing — review & editing, Investigation. **Yixing Li:** Writing — review & editing, Supervision. **Turtushikh Damba:** Writing — review & editing, Supervision. **Khongorzul Batchuluun:** Writing — review & editing, Supervision. **Yunxiao Liang:** Writing — review & editing, Supervision. **Lei Zhou:** Writing — review & editing, Writing — original draft, Visualization, Supervision, Resources, Project administration, Funding acquisition, Conceptualization.

ACKNOWLEDGEMENTS

This work was supported by National Key R&D Program of China (2023YFE0100800); Guangxi Science Foundation for Distinguished Young Scholars (2020GXNSFFA297008); Guangxi Natural Science Foundation (2019GXNSFDA245029); Guangxi Academy of Medical Sciences high-level Talents Foundation (YKY-GCRC-202302).

DECLARATION OF COMPETING INTEREST

The authors declare no competing interests.

DATA AVAILABILITY

Data will be made available on request.

APPENDIX A. SUPPLEMENTARY DATA

Supplementary data to this article can be found online at https://doi.org/10.1016/j.molmet.2024.101873.

REFERENCES

[1] Goossens GH. The metabolic phenotype in obesity: fat mass, body fat distribution, and adipose tissue function. Obes Facts 2017;10(3):207—15.
[2] Boulangé CL, Neves AL, Chilloux J, Nicholson JK, Dumas ME. Impact of the gut microbiota on inflammation, obesity, and metabolic disease. Genome Med 2016;8(1):42.
[3] Mohammed MS, Sendra S, Lloret J, Bosch I. Systems and WBANs for controlling obesity. J Healthc Eng 2018;2018:1564748.
[4] Tang QQ, Lane MD. Adipogenesis: from stem cell to adipocyte. Annu Rev Biochem 2012;81:715—36.
[5] Lefterova MI, Lazar MA. New developments in adipogenesis. Trends Endocrinol Metabol 2009;20(3):107—14.
[6] Vishvanath L, Gupta RK. Contribution of adipogenesis to healthy adipose tissue expansion in obesity. J Clin Invest 2019;129(10):4022—31.
[7] Reyes-Farias M, Fos-Domenech J, Serra D, Herrero L, Sánchez-Infantes D. White adipose tissue dysfunction in obesity and aging. Biochem Pharmacol 2021;192:114723.
[8] Cannon B, Nedergaard J. Brown adipose tissue: function and physiological significance. Physiol Rev 2004;84(1):277—359.
[9] Harms M, Seale P. Brown and beige fat: development, function and therapeutic potential. Natural Medicines 2013;19(10):1252—63.
[10] Li Y, Wang D, Ping X, Zhang Y, Zhang T, Wang L, et al. Local hyperthermia therapy induces browning of white fat and treats obesity. Cell 2022;185(6):949—966.e919.
[11] Wang QA, Tao C, Gupta RK, Scherer PE. Tracking adipogenesis during white adipose tissue development, expansion and regeneration. Natural Medicines 2013;19(10):1338—44.
[12] Kirichok Y, Krapivinsky G, Clapham DE. The mitochondrial calcium uniporter is a highly selective ion channel. Nature 2004;427(6972):360—4.
[13] Kamer KJ, Mootha VK. The molecular era of the mitochondrial calcium uniporter. Nat Rev Mol Cell Biol 2015;16(9):545—53.
[14] Woods JJ, Wilson JJ. Inhibitors of the mitochondrial calcium uniporter for the treatment of disease. Curr Opin Chem Biol 2020;55:9—18.
[15] Wang Y, Li X, Zhao F. *Mcu*-dependent mROS generation regulates cell metabolism and cell death modulated by the AMPK/PGC-1α/SIRT3 signaling pathway. Front Med 2021;8:674986.

[16] Glancy B, Balaban RS. Role of mitochondrial Ca2+ in the regulation of cellular energetics. Biochemistry 2012;51(14):2959–73.
[17] Lemasters JJ, Nieminen AL, Qian T, Trost LC, Elmore SP, Nishimura Y, et al. The mitochondrial permeability transition in cell death: a common mechanism in necrosis, apoptosis and autophagy. Biochim Biophys Acta 1998;1366(1–2):177–96.
[18] Tomar D, Jaña F, Dong Z, Quinn 3rd WJ, Jadiya P, Breves SL, et al. Blockade of *mcu*-mediated Ca(2+) uptake perturbs lipid metabolism via PP4-dependent AMPK dephosphorylation. Cell Rep 2019;26(13):3709–25.
[19] Tian S, Lei P, Zhang J, Sun Y, Li B, Shan Y. Sulforaphane balances Ca(2+) homeostasis injured by excessive fat via mitochondria-associated membrane (MAM). Mol Nutr Food Res 2021;65(14):e2001076.
[20] Wright LE, Vecellio Reane D, Milan G, Terrin A, Di Bello G, Belligoli A, et al. Increased mitochondrial calcium uniporter in adipocytes underlies mitochondrial alterations associated with insulin resistance. Am J Physiol Endocrinol Metab 2017;313(6):E641–50.
[21] Zhang Z, Luo Z, Yu L, Xiao Y, Liu S, Z AL, et al. Ruthenium 360 and mitoxantrone inhibit mitochondrial calcium uniporter channel to prevent liver steatosis induced by high-fat diet. Br J Pharmacol 2022;179(11):2678–96.
[22] Zhao X, Hu H, Wang C, Bai L, Wang Y, Wang W, et al. A comparison of methods for effective differentiation of the frozen-thawed 3T3-L1 cells. Anal Biochem 2019;568:57–64.
[23] Butler AA, Kozak LP. A recurring problem with the analysis of energy expenditure in genetic models expressing lean and obese phenotypes. Diabetes 2010;59(2):323–9.
[24] Tschöp MH, Speakman JR, Arch JR, Auwerx J, Brüning JC, Chan L, et al. A guide to analysis of mouse energy metabolism. Nat Methods 2011;9(1):57–63.
[25] Mouchiroud M, Camiré É, Aldow M, Caron A, Jubinville É, Turcotte L, et al. The Hepatokine TSK does not affect brown fat thermogenic capacity, body weight gain, and glucose homeostasis. Mol Metab 2019;30:184–91.
[26] Zhang Y, Fu Q, Wu T, Liu K, Xiao Y, Liao Q, et al. 5-Methoxyflavone ameliorates non-alcoholic fatty liver disease through targeting the cytochrome P450 1A1. Free Radical Biol Med 2023;195:178–91.
[27] Huang L, Liao Q, Pan T, Sun Y, Aluo Z, Xiao L, et al. Small intestine-specific knockout of CIDEC improves obesity and hepatic steatosis by inhibiting synthesis of phosphatidic acid. Int J Biol Sci 2022;18(15):5740–52.
[28] Li M, Xiao Y, Xiao L, Li Y, Jia M, Sun Y, et al. Epigoitrin alleviates lipid and glucose metabolic disorders induced by a high-fat diet. Food Funct 2022;13(13):7260–73.
[29] Lehrke M, Lazar MA. The many faces of PPARgamma. Cell 2005;123(6):993–9.
[30] Lane MD, Lin FT, MacDougald OA, Vasseur-Cognet M. Control of adipocyte differentiation by CCAAT/enhancer binding protein alpha (C/EBP alpha). Int J Obes Relat Metab Disord 1996;20(Suppl 3):S91–6.
[31] Kopelman PG. Obesity as a medical problem. Nature 2000;404(6778):635–43.
[32] Lu Q, Guo P, Liu A, Ares I, Martínez-Larrañaga MR, Wang X, et al. The role of long noncoding RNA in lipid, cholesterol, and glucose metabolism and treatment of obesity syndrome. Med Res Rev 2021;41(3):1751–74.
[33] Arruda AP, Hotamisligil GS. Calcium homeostasis and organelle function in the pathogenesis of obesity and diabetes. Cell Metabol 2015;22(3):381–97.
[34] Abeti R, Uzun E, Renganathan I, Honda T, Pook MA, Giunti P. Targeting lipid peroxidation and mitochondrial imbalance in Friedreich's ataxia. Pharmacol Res 2015;99:344–50.
[35] Pinto MC, Kihara AH, Goulart VA, Tonelli FM, Gomes KN, Ulrich H, et al. Calcium signaling and cell proliferation. Cell Signal 2015;27(11):2139–49.
[36] Min H, Kim W, Hong S, Lee S, Jeong J, Kim S, et al. Differentiation and homeostasis of effector Treg cells are regulated by inositol polyphosphates modulating Ca(2+) influx. Proc Natl Acad Sci USA 2022;119(27):e2121520119.
[37] Pinton P, Giorgi C, Siviero R, Zecchini E, Rizzuto R. Calcium and apoptosis: ER-mitochondria Ca2+ transfer in the control of apoptosis. Oncogene 2008;27(50):6407–18.
[38] Wang CH, Chen YF, Wu CY, Wu PC, Huang YL, Kao CH, et al. Cisd2 modulates the differentiation and functioning of adipocytes by regulating intracellular Ca2+ homeostasis. Hum Mol Genet 2014;23(18):4770–85.
[39] Rizzuto R, Marchi S, Bonora M, Aguiari P, Bononi A, De Stefani D, et al. Ca(2+) transfer from the ER to mitochondria: when, how and why. Biochim Biophys Acta 2009;1787(11):1342–51.
[40] Rizzuto R, De Stefani D, Raffaello A, Mammucari C. Mitochondria as sensors and regulators of calcium signalling. Nat Rev Mol Cell Biol 2012;13(9):566–78.
[41] Lemasters JJ, Theruvath TP, Zhong Z, Nieminen AL. Mitochondrial calcium and the permeability transition in cell death. Biochim Biophys Acta 2009;1787(11):1395–401.
[42] Brookes PS, Yoon Y, Robotham JL, Anders MW, Sheu SS. Calcium, ATP, and ROS: a mitochondrial love-hate triangle. Am J Physiol Cell Physiol 2004;287(4):C817–33.
[43] Ding L, Yang X, Tian H, Liang J, Zhang F, Wang G, et al. Seipin regulates lipid homeostasis by ensuring calcium-dependent mitochondrial metabolism. EMBO J 2018;37(17):e97572.
[44] Gao P, Jiang Y, Wu H, Sun F, Li Y, He H, et al. Inhibition of mitochondrial calcium overload by SIRT3 prevents obesity- or age-related whitening of Brown adipose tissue. Diabetes 2020;69(2):165–80.
[45] Xue K, Wu D, Wang Y, Zhao Y, Shen H, Yao J, et al. The mitochondrial calcium uniporter engages UCP1 to form a thermoporter that promotes thermogenesis. Cell Metabol 2022:1325–41.
[46] Flicker D, Sancak Y, Mick E, Goldberger O, Mootha VK. Exploring the in vivo role of the mitochondrial calcium uniporter in Brown fat bioenergetics. Cell Rep 2019;27(5):1364–1375.e1365.
[47] Ukropec J, Anunciado RP, Ravussin Y, Hulver MW, Kozak LP. UCP1-independent thermogenesis in white adipose tissue of cold-acclimated Ucp1-/- mice. J Biol Chem 2006;281(42):31894–908.
[48] Jeong SY, Seol DW. The role of mitochondria in apoptosis. BMB Rep 2008;41(1):11–22.
[49] Brand MD, Nicholls DG. Assessing mitochondrial dysfunction in cells. Biochem J 2011;435(2):297–312.
[50] Guan L, Che Z, Meng X, Yu Y, Li M, Yu Z, et al. *Mcu* Up-regulation contributes to myocardial ischemia-reperfusion Injury through calpain/OPA-1-mediated mitochondrial fusion/mitophagy Inhibition. J Cell Mol Med 2019;23(11):7830–43.
[51] Pittas K, Vrachatis DA, Angelidis C, Tsoucala S, Giannopoulos G, Deftereos S. The role of calcium handling mechanisms in reperfusion injury. Curr Pharmaceut Des 2018;24(34):4077–89.
[52] Liao Y, Hao Y, Chen H, He Q, Yuan Z, Cheng J. Mitochondrial calcium uniporter protein *Mcu* is involved in oxidative stress-induced cell death. Protein and Cell 2015;6(6):434–42.
[53] Chen CC, Kuo CH, Leu YL, Wang SH. Corylin reduces obesity and insulin resistance and promotes adipose tissue browning through SIRT-1 and β3-AR activation. Pharmacol Res 2021;164:105291.
[54] Forbes-Hernández TY, Cianciosi D, Ansary J, Mezzetti B, Bompadre S, Quiles JL, et al. Strawberry (Fragaria × ananassa cv. Romina) methanolic extract promotes browning in 3T3-L1 cells. Food Funct 2020;11(1):297–304.
[55] Andrikopoulos S, Blair AR, Deluca N, Fam BC, Proietto J. Evaluating the glucose tolerance test in mice. Am J Physiol Endocrinol Metab 2008;295(6):E1323–32.

